

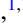

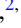




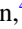



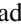




Evolution of the metallic state in $\text{LaNiO}_3/\text{LaAlO}_3$ superlattices measured by ^8Li β -detected NMR

Victoria L. Karner ^{1,2,*}, Aris Chatzichristos ^{2,3}, David L. Cortie ^{1,2,3,†}, Derek Fujimoto ^{2,3}, Robert F. Kiefl ^{2,3,4}, C. D. Philip Levy ⁴, Ruohong Li ⁴, Ryan M. L. McFadden ^{1,2,‡}, Gerald D. Morris ⁴, Matthew R. Pearson ⁴, Eva Benckiser ⁵, Alexander V. Boris ⁵, Georg Cristiani ⁵, Gennady Logvenov ⁵, Bernhard Keimer ⁵ and W. Andrew MacFarlane ^{1,2,4,§}

¹Department of Chemistry, University of British Columbia, Vancouver, British Columbia V6T 1Z1, Canada

²Stewart Blusson Quantum Matter Institute, University of British Columbia, Vancouver, British Columbia V6T 1Z4, Canada

³Department of Physics and Astronomy, University of British Columbia, Vancouver, British Columbia V6T 1Z1, Canada

⁴TRIUMF, 4004 Wesbrook Mall, Vancouver, British Columbia V6T 2A3, Canada

⁵Max Planck Institute for Solid State Research, 70569 Stuttgart, Germany



(Received 1 June 2021; revised 29 August 2021; accepted 27 October 2021; published 12 November 2021)

Using ion-implanted ^8Li β -detected NMR, we study the evolution of the correlated metallic state of LaNiO_3 in a series of $\text{LaNiO}_3/\text{LaAlO}_3$ superlattices as a function of bilayer thickness. Spin-lattice relaxation measurements in an applied field of 6.55 T reveal two equal amplitude components: one with metallic (T linear) $1/T_1$ and a second with a more complex T dependence. The metallic character of the slow relaxing component is only weakly affected by the LaNiO_3 thickness, while the fast component is much more sensitive, exhibiting the opposite temperature dependence (increasing toward low T) in the thinnest, most magnetic samples. The origin of this bipartite relaxation is discussed in terms of electronic phase separation.

DOI: [10.1103/PhysRevB.104.205114](https://doi.org/10.1103/PhysRevB.104.205114)

I. INTRODUCTION

The perovskite rare-earth metal nickelates ($R\text{NiO}_3$) are an important example of a metal-insulator transition (MIT) in a strongly correlated system [1]. The MIT can be tuned by increasing the size of the rare-earth metal cation R^{3+} which increases the Ni-O-Ni angle [1], and hence the electron hopping integral and conduction bandwidth. By this means, the MIT is suppressed to $T = 0$ K between $R = \text{Pr}$ and La . The prevailing view is that LaNiO_3 is a conventional metal characterized by a T^2 resistivity [2] with some evidence of strong correlations such as enhanced carrier mass and magnetic susceptibility. However, in superlattices (SLs) with insulating interlayers of LaAlO_3 , it can be driven insulating and antiferromagnetic when very thin [2 unit cells (u.c.)] [3,4], clearly demonstrating that LaNiO_3 remains close to quantum critical. This motivated the current experiment to better understand the correlated metallic state and how it changes as it approaches the thickness-controlled MIT.

NMR is an essential tool for studying strongly correlated electron materials, such as the high- T_c cuprates [5]; however, weak signals generally preclude its use for thin films, with a few important exceptions [6–11]. An alternative is β -detected NMR (β -NMR) [12], where a spin-polarized

radioisotope is implanted into the sample and the resulting β -decay is used to detect the NMR similar to muon spin rotation (μSR). β -NMR is a powerful local probe of metals [12], including strongly correlated Sr_2RuO_4 [13] and LaNiO_3 [14].

Here, β -NMR is used to study the evolution of the metallic state of LaNiO_3 with decreasing thickness in a series of $\text{LaNiO}_3/\text{LaAlO}_3$ SLs. Spin-lattice relaxation (SLR) measurements reveal two components: one with T linear relaxation below 200 K and a second with a more complex T dependence, indicating LaNiO_3 is not microscopically homogeneous but instead is phase separated. The slow relaxing component retains a metallic character similar to bulk LaNiO_3 , independent of thickness. In contrast, the fast relaxing component depends on thickness, deviates strongly from metallic, and exhibits a low T upturn, consistent with the emergence of magnetic ordering.

II. SAMPLES

Using pulsed laser deposition, the SLs were deposited on $(\text{LaAlO}_3)_{0.3}(\text{SrAlTaO}_6)_{0.7}$ (LSAT) substrates and annealed in an O_2 rich atmosphere, similar to the methods of Ref. [3]. The deposition begins with $n(=2, 3, 4, 10)$ u.c. of LaNiO_3 followed by an insulating interlayer of 2 u.c. of LaAlO_3 . The stacking sequence ($n||2$) was repeated 20 times for each SL (see Table I), terminating with LaAlO_3 . The crystallinity, interface sharpness, and layer thicknesses were verified using x-ray diffraction. Prior to the β -NMR experiments, the samples ($5 \times 5 \times 0.5$ mm³) were mounted on Al_2O_3 crystals with Ag paint for compatibility with the spectrometer's cold-finger cryostat. For further details on the sample characterization and growth, see the Supplemental Material [15].

*vkarn@chem.ubc.ca

†Present address: Institute for Superconducting and Electronic Materials, Australian Institute for Innovative Materials, University of Wollongong, North Wollongong, NSW 2500, Australia.

‡Present address: TRIUMF, 4004 Wesbrook Mall, Vancouver, BC V6T 2A3, Canada.

§wam@chem.ubc.ca

TABLE I. Summary of the superlattice samples.

n	Composition	Bilayer thickness	Total thickness
10	$[(\text{LaNiO}_3)_{10}(\text{LaAlO}_3)_2]_{20}$	4.6(5) nm	92(1) nm
4	$[(\text{LaNiO}_3)_4(\text{LaAlO}_3)_2]_{20}$	2.6(5) nm	52(1) nm
3	$[(\text{LaNiO}_3)_3(\text{LaAlO}_3)_2]_{20}$	2.0(5) nm	40(1) nm
2	$[(\text{LaNiO}_3)_2(\text{LaAlO}_3)_2]_{20}$	1.5(5) nm	30(1) nm

III. METHODS

To measure the β -NMR, a spin-polarized radioactive $^8\text{Li}^+$ ion beam was implanted into the sample. The measured β -decay asymmetry is proportional to the average longitudinal nuclear spin polarization [12,16], with a proportionality constant A_0 depending on the detector geometry and decay properties. The asymmetry was obtained by combining the count rates in two opposing scintillation detectors placed along the polarization axis. The experiments were performed at the ISAC facility at TRIUMF in Vancouver, Canada [12]. The NMR isotope ^8Li has nuclear spin $I = 2$, gyromagnetic ratio $\gamma/2\pi = 6.3016 \text{ MHz T}^{-1}$, nuclear electric quadrupole moment $Q = +32.6 \text{ mb}$, and radioactive lifetime $\tau = 1.21 \text{ s}$. The implantation energy was 4.9 keV, corresponding to a mean depth of $\sim 21 \text{ nm}$ with a straggle of 11 nm [17].

To measure the SLR, the asymmetry was monitored both during and after the 4 s beam pulse, during which it approaches a dynamic steady-state, while afterward it relaxes to near zero. Unlike conventional NMR, the ^8Li is hyperpolarized in flight by optical pumping, so no radio frequency (RF) field is required. The SLR rates were measured from 5 to 300 K in an applied field of $B_0 = 6.55 \text{ T}$ normal to the surface.

IV. RESULTS

Figure 1 compares the SLR data for different SLs. The relaxation is easily measurable in all cases. Generally, we expect it to be fastest in the (presumably most magnetic) $n = 2$ SL, and slower for the more metallic samples (larger n). To quantify its evolution, a model relaxation function is required. The simplest choice that provides a good fit is a biexponential, to which we add a nonrelaxing term to account for a small fraction of ^8Li stopping in the substrate due to range straggling. Specifically, at time t after an ^8Li arriving at time t' , the polarization follows

$$R(t, t') = f_{\text{SL}}[(1 - f_f)e^{-\lambda_s(t-t')} + f_f e^{-\lambda_f(t-t')}] + (1 - f_{\text{SL}}) \quad (1)$$

where λ_i ($i = s, f$) are the SLR rates. f_{SL} is the fraction of ^8Li in the SL, while $(1 - f_{\text{SL}})$ is in the substrate. Within the SL, f_f is the fast relaxing fraction and $(1 - f_f)$ is slow relaxing. The only T dependent parameters in the fits were the two rates. Biexponential relaxation appears intrinsic to ^8Li in LaNiO_3 , and a similar analysis was necessary for a bulk single crystal [14]. Interestingly, the fast relaxing fraction $f_f = 50\%$ is independent of LaNiO_3 thickness, and in agreement with the bulk

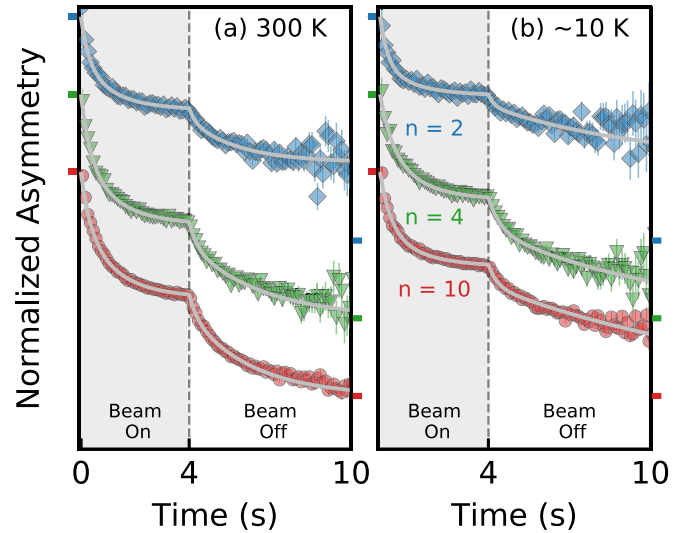


FIG. 1. Examples of $^8\text{Li}^+$ SLR data in $[(\text{LaNiO}_3)_n(\text{LaAlO}_3)_2]_{20}$ with $B_0 = 6.55 \text{ T}$ at two temperatures for $n = 2, 4$ and 10. The lines are fits to Eq. (1) convoluted with the 4 s beam pulse indicated by the shaded area. The data has been normalized and for clarity, offset vertically. The colored y-axis ticks on the left (right) represent the full (zero) asymmetry for each SL.

[14]. For further details on the analysis, see the Supplemental Material [15] (and Refs. [18–23] therein).

The resulting rates $(1/T_1)_i \equiv \lambda_i$ are shown as a function of temperature in Fig. 2. The slow rate in Fig. 2(a) remains linear (metallic) for all the SLs, with a slope similar to bulk LaNiO_3 [14]. Closer inspection reveals that (1) above $\sim 200 \text{ K}$ (marked by the vertical arrow), $1/T_1$ becomes sublinear; (2) the SLs are all faster relaxing than the bulk, and this enhancement is mostly due to a finite n -independent intercept as $T \rightarrow 0$; and (3) the slope changes systematically with n , but not monotonically, as the shallowest slope is at $n = 4$. Below 200 K, we fit $(1/T_1)_s$ to a line to obtain the values shown as a function of n in Fig. 3.

In contrast, the fast rate in Fig. 2(b) is much more strongly enhanced over the bulk (by a factor of 3–5 at 200 K). Similarly, there is a linear region (above $\sim 100 \text{ K}$), with a slope not far from the bulk, but this linearity does not persist to low T . Instead, it shows an upturn below 50 K, which is most dramatic at $n = 2$. At the MIT, we expect to lose the metallic Korringa relaxation, but as in other $R\text{NiO}_3$, the insulating state contains Ni local moments. The increasing SLR at low T is consistent with relaxation from fluctuations of the Ni spins which slow and eventually freeze.

Remarkably, we find no obvious signal from the LaAlO_3 . Like LSAT [24], the relaxation in bulk LaAlO_3 is extremely slow [25]. However, the LaAlO_3 is very thin, and any ^8Li at the interface will retain some coupling to the adjacent LaNiO_3 , enhancing $1/T_1$ compared to the bulk and making the distinctly LaAlO_3 volume fraction rather small. The $^8\text{Li}^+$ site energy in the LaAlO_3 layer may also be higher than LaNiO_3 due to the higher valent Al^{3+} , resulting in a bias against stopping in this layer. In the thin SLs, the LaAlO_3 fraction may be included in the substrate term, while in the

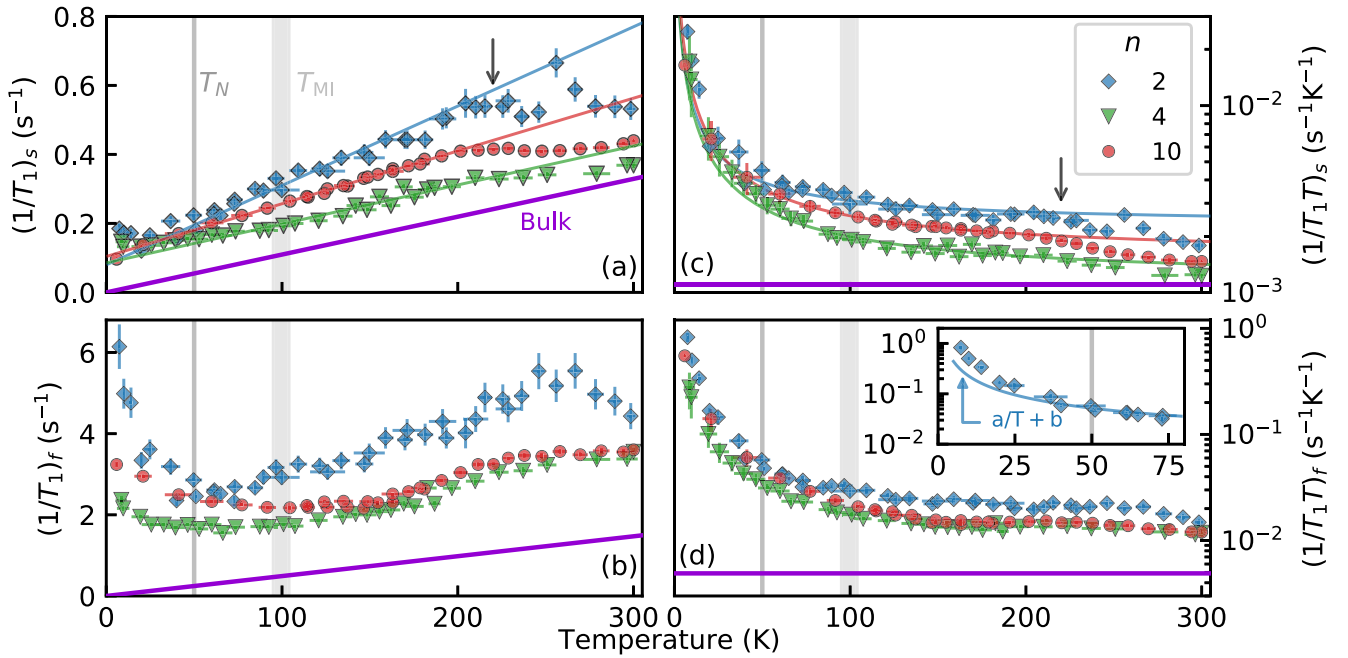


FIG. 2. The slow [(a), (c)] and fast [(b), (d)] ^8Li SLR rates and $(T_1T)^{-1}$ as a function of temperature at $B_0 = 6.55\text{ T}$ in $[(\text{LaNiO}_3)_n(\text{LaAlO}_3)_{20}]_{20}$ for $n = 2, 4,$ and 10 . Below $\sim 200\text{ K}$, $(1/T_1)_s$ appears linear with a nonzero intercept (fits shown with solid lines). The vertical arrow at $\sim 200\text{ K}$ indicates the sublinear deviation. The shaded region and the vertical line illustrate the reported T_{MI} and T_N in an $n = 2$ SL on SrTiO_3 [3]. For reference, the bulk Korringa slope is shown as the solid purple line [14]. The inset of panel (d) illustrates the low T upturn for $n = 2$, which spans more than an order of magnitude. The data for the $n = 3$ SL has been omitted to avoid clutter; however, the trend is very similar to $n = 2$.

thicker SLs it may make a small contribution to the slow component.

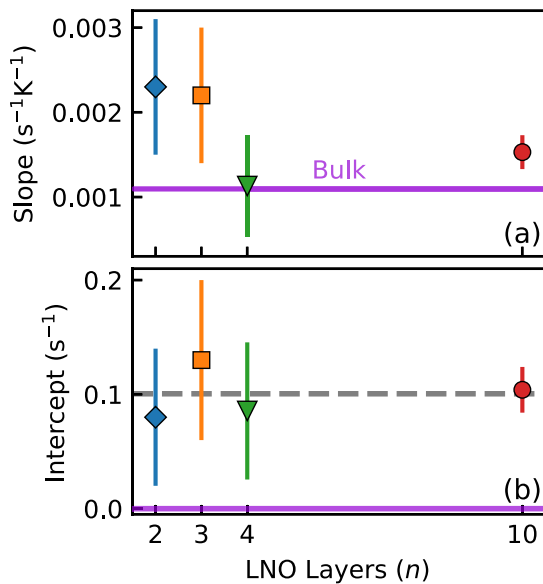


FIG. 3. (a) Slopes from the linear region of the slow component as a function of the LaNiO_3 thickness n . The bulk slope is shown as the solid purple line. The $n = 4$ and 10 values are scattered around the bulk, while the thinner SLs ($n = 2$ and 3) are significantly enhanced. (b) The $T \rightarrow 0$ intercepts appear independent of n , with average value shown by the dashed grey line.

V. DISCUSSION

Having outlined the results, we now discuss their implications. Like the implanted muon in μSR , $^8\text{Li}^+$ is typically located at a high-symmetry interstitial site in the host lattice. In perovskite oxides, this site (denoted P) is midway between adjacent A -site ions at the center of a square BO plaquette [14,24,26]. Analogous to the implanted muon and native NMR nuclei, ^8Li is coupled via the hyperfine interaction to the electronic system of the host. However, it is much longer lived than the muon, making it sensitive to phenomena on longer timescales such as Korringa relaxation.

With only one site, biexponential relaxation is unexpected. In bulk LaNiO_3 , where both rates are T linear, we attributed it to two subtly different P sites in an unconventional distorted perovskite structure [14]. This was reasonable, since the rates differed only in magnitude, not temperature dependence. However, it is incompatible with the present data where they exhibit distinct T dependences. With no evidence for other sites, we instead propose that the electronic state of LaNiO_3 (even in a metallic single crystal) is *intrinsically inhomogeneous*, i.e., microscopically separated into two equally abundant phases with distinct electronic properties. Electronic phase separation is prevalent in many correlated electron conductors [27], including stripe order in the closely related (but 2D) hole-doped La_2NiO_4 [28]; however, this is the first evidence for it in a 3D perovskite metal.

Separation into distinct metallic states is rather uncommon, but it does occur in the Kondo lattice compound YbRh_2Si_2 , where ^{29}Si spin-lattice relaxation becomes biexponential near the field-induced quantum critical point [29]. Interestingly,

here, the phase fraction (and not the relaxation rate) evolves with magnetic field and temperature, but converges toward $f_f = 0.5$ ($R = 1$ in their notation) at the lowest temperatures. LaNiO_3 has been suggested to have a Kondo lattice character with a much larger energy scale [30]. The phase separation revealed in our data persists at least up to 300 K, even in the single crystal. So, unlike YbRh_2Si_2 , where the phenomenon is limited to low T , we expect lattice dynamics to have some influence.

In contrast, phase separation into metallic and insulating phases is known in other RNiO_3 [31,32], but only in the vicinity of the MIT. There, the insulating volume fraction varies from 0 to 1 through a narrow coexistence region around the transition. In contrast, our volume fraction is constant over the whole temperature range, including in the metallic limit of the single crystal [14]. If this phenomenon is related, then the metal-insulator phase separation must reflect some underlying inhomogeneity present in the high-temperature metallic phase. This is likely structural in origin. This is observed, for example, in NdNiO_3 , where the formation of insulating regions is correlated with step-edges in the sample and the microstructure of this phase separation is stable through temperature cycling [31]. Candidate sources of structural heterogeneity are competing distorted perovskite structures (octahedral rotation pattern) or bond disproportionation (octahedral size) [1,33]. We note the precise structure of LaNiO_3 remains elusive. Although it is considered rhombohedral, recent neutron scattering results indicate a lower local symmetry [34,35]. It has also been suggested to contain nanoscopic monoclinic insulating pockets [34], which is inconsistent with the two distinct metallic phases we find in bulk [14].

In summary, the biexponential relaxation strongly suggests *microscopic electronic phase separation* in LaNiO_3 that persists up to at least 300 K. The phase separation is static on the second timescale, robust across multiple LaNiO_3 samples, including a single crystal [14], thin film [14], and SLs, and has not yet been observed with other experimental techniques. Confirming it may require other local probes, such as conventional NMR, or scanning probe methods that could directly image its spatial distribution [32].

In similar SLs, low energy μSR (in zero and low fields) finds a broad distribution of static fields (150 G width) below 50 K at $n = 2$ which pervade the entire sample volume [3], seemingly inconsistent with our results. However, $1/T_1$ does not probe the static fields directly, instead being determined by field fluctuations at the Larmor frequency (41.27 MHz). On the other hand, static fields could propagate out from an incomplete magnetic volume fraction into the nonmagnetic phase, provided the two were intimately mixed at the nanoscale [36]. This may explain why the scale of the internal fields is more than $10\times$ smaller than bulk RNiO_3 [37]. Alternatively, in analogy with YbRh_2Si_2 , we may have stabilized a distinct phase-separated ground state with the large B_0 field.

Now we turn to what the evolution of $1/T_1$ can tell us about the MIT at small n . In a conventional metal, the Korringa T linear dependence is a consequence of Fermi statistics and a density of states (DOS) that is smooth and featureless on the scale of kT . The Korringa slope is then proportional to the square of the DOS at the Fermi level $\rho(E_F)$. Considering

Fig. 3(a), there is a twofold increase in the slow component's slope for $n < 4$, consistent with an effective narrowing of the conduction band on approaching the 2D limit. However, for all n , we find a finite intercept, inconsistent with simple metallic behavior. More generally, for a correlated metal susceptible to magnetic order, the Moriya expression [38] relates $1/T_1$ to the imaginary part of the generalized susceptibility $\chi(\mathbf{q}, \omega)$,

$$\frac{1}{T_1 T} = \frac{4k_B}{\hbar} \sum_{\mathbf{q}} \frac{|A(\mathbf{q})|^2}{(\gamma_e \hbar)^2} \frac{1}{\hbar \omega_0} \chi''(\mathbf{q}, \omega_0), \quad (2)$$

where γ_e is the electron gyromagnetic ratio, ω_0 is the NMR frequency, and $A(\mathbf{q})$ is the hyperfine form factor which acts as a filtering function on magnetic fluctuations at wave vector \mathbf{q} . For a conventional metal, the summation in Eq. (2) is independent of T for $kT \ll E_F$. A finite intercept implies that, in addition to a constant part, the sum contains a term proportional to $1/T$. This is seen clearly in the corresponding plot of $1/(T_1 T)$ (on a log scale) in Fig. 2(c). Such a Curie-like term suggests a population of dilute uncoupled local moments, as has been considered near the MIT in doped semiconductors [39]; however, we find no evidence for the emergence, at low temperature, of a broad distribution of $1/T_1$ that should arise from dilute spins. Interestingly, this term appears independent of n , so it is probably not caused by Ni moments at the LaAlO_3 interface.

Aside from the intercept, the slow relaxing phase exhibits a metallic character that is not very strongly modified from the bulk, even for the smallest n . In contrast, the fast relaxing phase exhibits a much more dramatic sensitivity to thickness. In the bulk, the factor of 4 between the Korringa slopes in the fast and slow phases [14] would imply a factor of 2 in $\rho(E_F)$ in an uncorrelated metal. In the SLs, compared to the slow component, $(1/T_1)_f$ shows a $10\times$ larger T independent term (vertical shift) and an upturn below ~ 50 K with $(1/T_1)_f$ doubling between 50 K and 4 K at $n = 2$ [inset of Fig. 2(d)]. Similar $n = 2$ SLs have a zero-field Néel transition at $T_N \approx 50$ K [3,4] near the upturn and an ordering wave vector $\mathbf{q}_{\text{AF}} = (1/4, 1/4, 1/4)$ [4]. The P site hyperfine form factor $A(\mathbf{q}_{\text{AF}}) \neq 0$, so ^7Li senses fluctuations at \mathbf{q}_{AF} . However, even the thicker SLs with $n = 4$ and 10 (that are thought to remain nonmagnetic and metallic) show a similar, albeit muted feature. The upturn implies a term in Eq. (2) increasing more steeply than $1/T$ at low T . This is likely related to magnetic ordering, but probably modified by the strong applied field (cf. the transition in Mn-doped Bi_2Te_3 [40]). Note the vertical scale in Fig. 2(d) spans an order of magnitude more range than the slow component in Fig. 2(c).

Finally, we return to the sublinearity in $(1/T_1)_s$ above 200 K (vertical arrow in Fig. 2). The deviation is subtle, sample dependent, and does not vary monotonically with n , as it is smallest at $n = 4$. A similar deviation was observed in bulk LaNiO_3 , although there it had the opposite sense for the slow and fast components. This feature is probably related to small changes in the Ni—O—Ni angle around 200 K [34], which also coincides with a decrease in the carrier density from RF conductivity [35]. In addition, the magnetic susceptibility crosses over from a low temperature Pauli-like regime to a high temperature Curie-Weiss dependence [41] at about

200 K. It is reasonable to expect such a small structural change would differ between a crystal, SL, and film, and it may even depend on the precise thermal history.

VI. CONCLUSION

β -NMR spin-lattice relaxation measurements of implanted ^8Li in a series of $\text{LaNiO}_3/\text{LaAlO}_3$ SLs reveal biexponential relaxation, consistent with single crystal LaNiO_3 [14]; but, in contrast, the two components exhibit very different temperature dependences. Thus, we propose LaNiO_3 is electronically phase separated. The slow relaxing phase is metallic, not strongly modified from the bulk, and persists to low T , even for the thinnest ($n = 2$) SL. As $n \rightarrow 2$, the slope and the

DOS are enhanced consistent with band narrowing toward the 2D limit. In contrast, the fast relaxing phase is much more sensitive to n and appears magnetic at low T . Any microscopic understanding of the electronic properties of LaNiO_3 and its MIT in SLs must take this phase separation into account.

ACKNOWLEDGMENTS

We thank R. Abasalti, D. J. Arseneau, S. Daviel, B. Hitti, and D. Vyas for technical assistance. We thank A. Frano, S. Johnston, Q. Si, and M. Vojta for useful discussions. This work was supported by NSERC Canada. Work at the MPI-FKF (sample synthesis and characterization) was supported by the Deutsche Forschungsgemeinschaft (DFG, German Research Foundation) Projektnummer 107745047-TRR 80.

-
- [1] S. Catalano, M. Gibert, J. Fowlie, J. Íñiguez, J.-M. Triscone, and J. Kreisel, Rare-earth nickelates RNiO_3 : Thin films and heterostructures, *Rep. Prog. Phys.* **81**, 046501 (2018).
- [2] J.-S. Zhou, L. G. Marshall, and J. B. Goodenough, Mass enhancement versus Stoner enhancement in strongly correlated metallic perovskites: LaNiO_3 and LaCuO_3 , *Phys. Rev. B* **89**, 245138 (2014).
- [3] A. V. Boris, Y. Matiks, E. Benckiser, A. Frano, P. Popovich, V. Hinkov, P. Wochner, M. Castro-Colin, E. Detemple, V. K. Malik, C. Bernhard, T. Prokscha, A. Suter, Z. Salman, E. Morenzoni, G. Cristiani, H.-U. Habermeier, and B. Keimer, Dimensionality control of electronic phase transitions in nickel-oxide superlattices, *Science* **332**, 937 (2011).
- [4] A. Frano, E. Schierle, M. W. Haverkort, Y. Lu, M. Wu, S. Blanco-Canosa, U. Nwankwo, A. V. Boris, P. Wochner, G. Cristiani, H. U. Habermeier, G. Logvenov, V. Hinkov, E. Benckiser, E. Weschke, and B. Keimer, Orbital Control of Noncollinear Magnetic Order in Nickel Oxide Heterostructures, *Phys. Rev. Lett.* **111**, 106804 (2013).
- [5] R. E. Walstedt, Introduction to NMR studies of metals, metallic compounds, and superconductors, in *The NMR Probe of High-Tc Materials* (Springer, Berlin, 2008), pp. 13–65.
- [6] M. Yudkowsky, W. P. Halperin, and Ivan K. Schuller, Nuclear-magnetic-resonance study of electronic structure in the copper-niobium superlattice, *Phys. Rev. B* **31**, 1637 (1985).
- [7] G. Zheng, Y. Kitaoka, Y. Oda, K. Asayama, Y. Obi, H. Fujimori, and R. Aoki, Proximity effect-induced superconductivity and NMR relaxation in Nb-Cu multilayers, *J. Phys. Soc. Jpn* **60**, 599 (1991).
- [8] C. Mény, P. Panissod, and R. Loloee, Structural study of cobalt-copper multilayers by NMR, *Phys. Rev. B* **45**, 12269 (1992).
- [9] Q. Y. Jin, Y. B. Xu, H. R. Zhai, C. Hu, M. Lu, Q. S. Bie, Y. Zhai, G. L. Dunifer, R. Naik, and M. Ahmad, Direct Evidence of Spin Polarization Oscillations in the Cu Layers of Fe/Cu Multilayers Observed by NMR, *Phys. Rev. Lett.* **72**, 768 (1994).
- [10] T. Yamanaka, M. Shimozawa, R. Endo, Y. Mizukami, H. Shishido, T. Terashima, T. Shibauchi, Y. Matsuda, and K. Ishida, Interface between heavy fermions and normal electrons investigated by spatially resolved nuclear magnetic resonance, *Phys. Rev. B* **92**, 241105(R) (2015).
- [11] G. Nakamine, T. Yamanaka, S. Kitagawa, M. Naritsuka, T. Ishii, T. Shibauchi, T. Terashima, Y. Kasahara, Y. Matsuda, and K. Ishida, Modification of magnetic fluctuations by interfacial interactions in artificially engineered heavy-fermion superlattices, *Phys. Rev. B* **99**, 081115(R) (2019).
- [12] W. A. MacFarlane, Implanted-ion β NMR: A new probe for nanoscience, *Solid State Nucl. Magn. Reson.* **68–69**, 1 (2015).
- [13] D. L. Cortie, T. Buck, M. H. Dehn, R. F. Kiefl, C. D. P. Levy, R. M. L. McFadden, G. D. Morris, M. R. Pearson, Z. Salman, Y. Maeno, and W. A. MacFarlane, Spin fluctuations in the exotic metallic state of Sr_2RuO_4 studied with β -NMR, *Phys. Rev. B* **91**, 241113(R) (2015).
- [14] V. L. Karner, A. Chatzichristos, D. L. Cortie, M. H. Dehn, O. Foyevtsov, K. Foyevtsova, D. Fujimoto, R. F. Kiefl, C. D. P. Levy, R. Li, R. M. L. McFadden, G. D. Morris, M. R. Pearson, M. Stachura, J. O. Ticknor, G. Cristiani, G. Logvenov, F. Wrobel, B. Keimer, J. Zhang *et al.*, Local metallic and structural properties of the strongly correlated metal LaNiO_3 using ^8Li β -NMR, *Phys. Rev. B* **100**, 165109 (2019).
- [15] See Supplemental Material at <http://link.aps.org/supplemental/10.1103/PhysRevB.104.205114> for more information on the sample growth and characterization, and the data analysis.
- [16] H. Ackermann, P. Heitjans, and H.-J. Stöckmann, β emitters and isomeric nuclei as probes in condensed matter, in *Hyperfine Interactions of Radioactive Nuclei*, Topics in Current Physics Vol. 31, edited by J. Christiansen (Springer, Berlin, 1983), Chap. 6, pp. 291–361.
- [17] J. F. Ziegler, M. D. Ziegler, and J. P. Biersack, SRIM, the stopping and range of ions in matter, *Nucl. Instrum. Methods Phys. Res., Sect. B* **268**, 1818 (2010).
- [18] E. R. Andrew and D. P. Tunstall, Spin-lattice relaxation in imperfect cubic crystals and in non-cubic crystals, *Proc. Phys. Soc. London* **78**, 1 (1961).
- [19] F. James and M. Roos, MINUIT—a system for function minimization and analysis of the parameter errors and correlations, *Comput. Phys. Commun.* **10**, 343 (1975).
- [20] A. F. McDowell, Magnetization-recovery curves for quadrupolar spins, *J. Magn. Reson., Ser. A* **113**, 242 (1995).
- [21] R. Brun and F. Rademakers, ROOT—an object oriented data analysis framework, *Nucl. Instrum. Methods Phys. Res., Sect. A* **389**, 81 (1997).

- [22] W. A. MacFarlane, C. D. P. Levy, M. R. Pearson, T. Buck, K. H. Chow, A. N. Hariwal, R. F. Kiefl, F. H. McGee, G. D. Morris, and D. Wang, The initial state of optically polarized $^8\text{Li}^+$ from the β -NMR in bismuth, *J. Phys.: Conf. Ser.* **551**, 012059 (2014).
- [23] C. D. P. Levy, M. R. Pearson, R. F. Kiefl, E. Mané, G. D. Morris, and A. Voss, Laser polarization facility, *Hyperfine Interact.* **225**, 165 (2014).
- [24] V. L. Karner, R. M. L. McFadden, M. H. Dehn, D. Fujimoto, A. Chatzichristos, G. D. Morris, M. R. Pearson, C. D. P. Levy, A. Reisner, L. H. Tjeng, R. F. Kiefl, and W. A. MacFarlane, Beta-detected NMR of LSAT and YSZ, *JPS Conf. Proc.* **21**, 011024 (2018).
- [25] V. L. Karner, R. M. L. McFadden, A. Chatzichristos, G. D. Morris, M. R. Pearson, C. D. P. Levy, Z. Salman, D. L. Cortie, R. F. Kiefl, and W. A. MacFarlane, Beta detected NMR of LaAlO_3 , *JPS Conf. Proc.* **21**, 011023 (2018).
- [26] W. A. MacFarlane, G. D. Morris, K. H. Chow, R. A. Baartman, S. Daviel, K. M. Nichol, R. Poutissou, E. Dumont, L. H. Greene, and R. F. Kiefl, Quadrupolar split ^8Li β -NMR in SrTiO_3 , *Phys. B: Condens. Matter* **326**, 209 (2003).
- [27] M. Liu, A. J. Sternbach, and D. N. Basov, Nanoscale electro-dynamics of strongly correlated quantum materials, *Rep. Prog. Phys.* **80**, 014501 (2016).
- [28] Y. Shen, G. Fabbri, H. Miao, Y. Cao, D. Meyers, D. G. Mazzone, T. A. Assefa, X. M. Chen, K. Kisslinger, D. Prabhakaran, A. T. Boothroyd, J. M. Tranquada, W. Hu, A. M. Barbour, S. B. Wilkins, C. Mazzoli, I. K. Robinson, and M. P. M. Dean, Charge Condensation and Lattice Coupling Drives Stripe Formation in Nickelates, *Phys. Rev. Lett.* **126**, 177601 (2021).
- [29] S. Kambe, H. Sakai, Y. Tokunaga, G. Lapertot, T. D. Matsuda, G. Knebel, J. Flouquet, and R. E. Walstedt, Degenerate Fermi and non-Fermi liquids near a quantum critical phase transition, *Nat. Phys.* **10**, 840 (2014).
- [30] V. I. Anisimov, D. Bukhvalov, and T. M. Rice, Electronic structure of possible nickelate analogs to the cuprates, *Phys. Rev. B* **59**, 7901 (1999).
- [31] G. Mattoni, P. Zubko, F. Maccherozzi, A. J. H. van der Torren, D. B. Boltje, M. Hadjimichael, N. Manca, S. Catalano, M. Gibert, Y. Liu, J. Aarts, J.-M. Triscone, S. S. Dhesi, and A. D. Caviglia, Striped nanoscale phase separation at the metal-insulator transition of heteroepitaxial nickelates, *Nat. Commun.* **7**, 13141 (2016).
- [32] D. Preziosi, L. Lopez-Mir, X. Li, T. Cornelissen, J. H. Lee, F. Trier, K. Bouzehouane, S. Valencia, A. Gloter, A. Barthélémy, and M. Bibes, Direct mapping of phase separation across the metal-insulator transition of NdNiO_3 , *Nano Lett.* **18**, 2226 (2018).
- [33] J. A. Alonso, J. L. García-Muñoz, M. T. Fernández-Díaz, M. A. G. Aranda, M. J. Martínez-Lope, and M. T. Casais, Charge Disproportionation in RNiO_3 Perovskites: Simultaneous Metal-Insulator and Structural Transition in YNiO_3 , *Phys. Rev. Lett.* **82**, 3871 (1999).
- [34] B. Li, D. Louca, S. Yano, L. G. Marshall, J. Zhou, and J. B. Goodenough, Insulating pockets in metallic LaNiO_3 , *Adv. Electron. Mater.* **2**, 1500261 (2015).
- [35] J. Shamblyn, M. Heres, H. Zhou, J. Sangoro, M. Lang, J. Neuefeind, J. A. Alonso, and S. Johnston, Experimental evidence for bipolaron condensation as a mechanism for the metal-insulator transition in rare-earth nickelates, *Nat. Commun.* **9**, 86 (2018).
- [36] H.-J. Grafe, P. Lepucki, M. Witschel, A. P. Dioguardi, R. Kappenberger, S. Aswartham, S. Wurmehl, and B. Büchner, Unified phase diagram of F-doped LaFeAsO by means of NMR and NQR parameters, *Phys. Rev. B* **101**, 054519 (2020).
- [37] B. A. Frandsen, L. Liu, S. C. Cheung, Z. Guguchia, R. Khasanov, E. Morenzoni, T. J. S. Munsie, A. M. Hallas, M. N. Wilson, Y. Cai, G. M. Luke, B. Chen, W. Li, C. Jin, C. Ding, S. Guo, F. Ning, T. U. Ito, W. Higemoto, S. J. L. Billinge *et al.*, Volume-wise destruction of the antiferromagnetic Mott insulating state through quantum tuning, *Nat. Commun.* **7**, 12519 (2016).
- [38] T. Moriya, The effect of electron-electron interaction on the nuclear spin relaxation in metals, *J. Phys. Soc. Jpn.* **18**, 516 (1963).
- [39] Z.-Z. Gan and P. A. Lee, Nuclear-spin relaxation near the metal-insulator transition, *Phys. Rev. B* **33**, 3595 (1986).
- [40] R. M. L. McFadden, A. Chatzichristos, D. L. Cortie, D. Fujimoto, Y. S. Hor, H. Ji, V. L. Karner, R. F. Kiefl, C. D. P. Levy, R. Li, I. McKenzie, G. D. Morris, M. R. Pearson, M. Stachura, R. J. Cava, and W. A. MacFarlane, Local electronic and magnetic properties of the doped topological insulators Bi_2Se_3 : Ca and Bi_2Te_3 : Mn investigated using ion-implanted ^8Li β -NMR, *Phys. Rev. B* **102**, 235206 (2020).
- [41] J. Zhang, H. Zheng, Y. Ren, and J. F. Mitchell, High-pressure floating-zone growth of perovskite nickelate LaNiO_3 single crystals, *Cryst. Growth Des.* **17**, 2730 (2017).